Survey: Automatic Recognition of Musculoskeletal Disorders from Radiographs

Mennatallah M Abdel Aal
Faculty of Computer Science
Misr International University
Email: mennatallah1500885@miuegypt.edu.eg

Sara H Awwad
Faculty of Computer Science
Misr International University
Email: sara1502749@miuegypt.edu.eg

Farah H Ahmed
Faculty of Computer Science
Misr International University
Email: farah1502451@miuegypt.edu.eg

Amira G Wasfi
Faculty of Computer Science
Misr International University
Email: amira1504361@miuegypt.edu.eg

Taraggy M Ghanim
Faculty of Computer Science
Misr International University
Email: taraggy.ghanim@miuegypt.edu.eg

Ayman M Nabil
Faculty of Computer Science
Misr International University
Email: ayman.nabil@miuegypt.edu.eg

***Abstract*—Automatic Recognition of Musculoskeletal Disorders is one of the important applications of computers in clinical medicine. Radiographs must be classified as normal or abnormal. There is a critical need for fast and inexpensive but reliable automatic classification systems should be satisfied. It is desired to discriminate between the various types of musculoskeletal disorders. Different approaches have been proposed recently in the field of pattern-recognition. Our proposed paper introduces a detailed survey on up-to-date published papers specialized in this point of research.**

***Index Terms*—Musculoskeletal disorders,Radiography, Pattern recognition**

I. INTRODUCTION

Musculoskeletal disorders (MSDs) are becoming one of the most important health concerns. MSDs affect more than 1.7 billion people worldwide [1], and treatment is quite expensive and misdiagnosis may cause severe problems. MSDs are conditions that affect bones, joints and muscles. Different types of MSDs include tendinitis, carpal tunnel syndrome, osteoarthritis, rheumatoid arthritis and fibromyalgia and bone fractures [2]. Some of these types as shown in Fig.1. Musculoskeletal imaging through

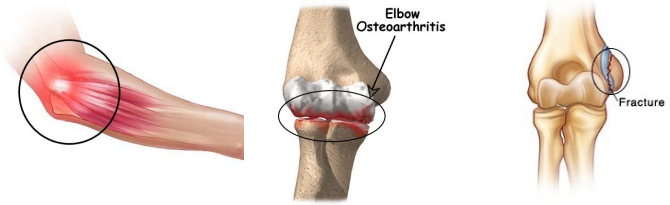

(a) Tendinitis (b) Osteoarthritis (c) Bone Fracture

Fig. 1: Common Musculoskeletal Disorders

radiographs involves acquisition, analysis and decision making. This can be applied on different musculoskeletal organs like bones, joints or even soft tissues due to injury. The automatic diagnosis of disorders serves treatment and helps in planning therapy and support interventional guidance.

Recently the need of advanced computational methods that help in the diagnosis of MSDs has been increasing. Given a system that can automatically detect whether a radiograph is normal or abnormal, would help work-flow and also the patients to be treated faster. It can also help reduce the workload on radiologists, which would mean less fatigue and thus diagnose a case more accurately. Automatic Recognition systems can help clinicians and researchers to introduce the commonness and occurrence rates, and would aid in determining the impact of disorders and their prognosis. It is stated that the reached automatic detection of abnormalities is still not equivalent to the best radiologists [2]. Medical images might produce noisy captures, which could affect the reliability of the results or hide any musculoskeletal conditions ([3], [4]). Some studies required manual interactions which was time-consuming, laborious and erring ([5], [6]) .

Our survey paper is organized as follows: section 2 provides medical background and some recently proposed medical researches, section 3 summarizes some recent proposed technical systems that serve our point of research, section 4 shows the popular databases of different types of MSD disorders, section 5 proposes a comparative study between the experiments of all the mentioned systems, and finally section 6 gives the conclusion of our proposed survey paper.

II. MEDICAL BACKGROUND

Some medical researches provide useful medical background that may be helpful in constructing automatic systems. An approach used the expertise of clinicians to develop a system to classify musculoskeletal disorders in upper-limbs [7]. Another approach was to detect abnormalities in knee articular cartilage in MRI images [8]. Plain radio-graphs or computed tomography are used for diagnosing vertebral fracture based on the height of the vertebrae [9]. Another approach for vertebral segmentation introduced a framework

for localizing lumbar in vertebral bodies in CT scans [10]. A study determines rate of missed musculoskeletal findings reported from trauma CT scans in order to evaluate the importance of these missed findings. [11]

III. Literature Reviews

Introduced papers in this field are divided into three main categories; classification systems, segmentation based systems and 3D constructions and architectures, as described in details in this section.

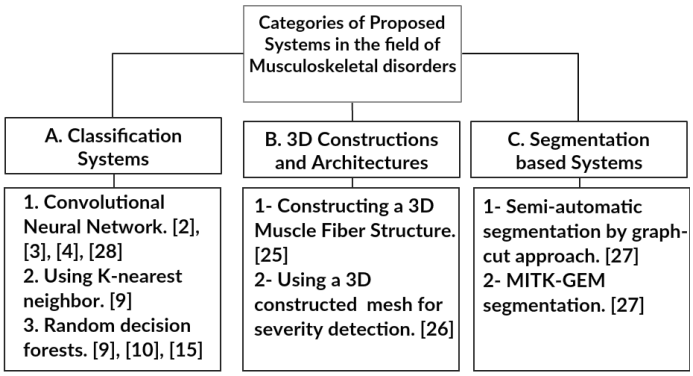

Fig. 2: Categories of proposed systems in the field of musculoskeletal disorders

A. *Classification*

1) "MURA: Large Dataset for Abnormality Detection in Musculoskeletal Radiographs": The model's pipeline acquires one or more views for the area of interest as input [2]. For every view, a 169 layered convolutional neural network (CNN) anticipates the probability of anomalies which could be detected, using the arithmetic mean of the anomalies probabilities from CNN as shown in Fig. 3. The weights of

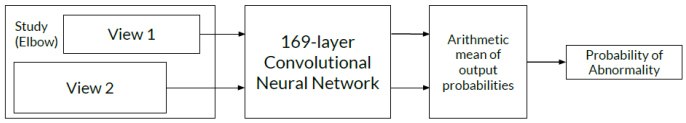

Fig. 3: MURA's model

the network were initialized with weights from a pre-trained model on ImageNet [12]. For pre-processing the input, each image is normalized to be similar to the ImageNet training data-set. Images are then scaled to 320 x 320, afterwards, augmentation is performed on the data by random lateral inversions up to 30 degrees.

A Dense Convolutional Network architecture was utilized by the network which is essential in connecting each layer to anticipate results beforehand. The final fully connected layer was substituted by a layer that has a single output, followed by applying a sigmoid non-linearity.

2) "Automatic Knee Osteoarthritis Diagnosis from Plain Radiographs: A Deep Learning-based Approach": A Deep Siamese architecture was proposed depending on convolutional neural network (CNN). Knee osteoarthritis (OA) is detected and Kellgren Lawrence (KL) method was applied to decide severity level [13]. In the design of the CNN, a small convolutional stack filters of 3x3 is used. Three models are trained with three different seeds. Predictions are summed and transferred to Softmax layer for normalization. Probability of KL j grade of image x out of k classes is defined by equation 1.

$$P(y=j|\mathbf{x}) = \frac{\exp\left[\sum_{m=1}^{M} \hat{P}_m(y=j|\mathbf{x})\right]}{\exp\left[\sum_{k=1}^{K}\sum_{m=1}^{M} \hat{P}_m(y=k|\mathbf{x})\right]} \quad (1)$$

3) "Shape-Aware Deep Convolutional Neural Network for Vertebrae Segmentation": The UNet architecture is performed for extracting different objects [4]. This was achieved in CNN by contracting the path to reduce the input size from 64x64 to 8x8 and another expanding path. Nine convolutional layers were applied per contracting path. Batch normalization and rectified linear unit layer were then applied. In addition to the 9 layers, another three 2x2 pooling layers were applied. One pooling layer was preceded by two convolutional layers. The proposed approach achieved up-sampling then concatenation between data in the expanding path and its corresponding data in the contracting path. A single channel vertebra patch of size 64x64 is extracted by the network, and a two probabilistic output model is used for the prediction of the same vertebra mask. The network has 24,238,210 parameters. A dataset having (x)- segmentation label (y) pairs, with a set of W parameters. This set of parameters aim to minimize a loss function Lt. The pixel-wise log loss, which was the loss function form and was updated and extended and needed for segmentation, as shown in equation 2

$$\hat{W} = \underset{\mathbf{W}}{arg\,min} \sum_{n=1}^{N} (L_t(\{x^{(n)}, y^{(n)}\}; W) + L_s(\{x^{(n)}, y^{(n)}\}; W)) \quad (2)$$

Where N represents number of training samples, while $x(n), y(n)$ is the n-th training sample with its corresponding manual segmentation. The pixel-wise segmentation loss per sample was computed by equation 3.

$$L_t = (\{x, y\}; W) = -\sum_{i \epsilon \Omega_p} \sum_{j=1}^{M} y_i^j \log P(y_i^j = 1|x_i; W), \quad (3)$$

$$P(y_i^j = 1|x_i; W) = \frac{\exp(a_j(x_i))}{\sum_{k=1}^{M} exp(a_k(x_i))}$$

A novel shape-based term, Ls, was introduced for the training of the segmentation network. The network produced prediction

masks from the training vertebral shapes which were then used to predict objects as shown in equation 4.

$$L_s(\{x,y\};W) = -\sum_{i \epsilon \hat{\Omega}_p} \sum_{j=1}^{M} y_i^j E_i \log P(y_i^j = 1 | x_i; W); E_i = D(\hat{C}, C_{GT}) \tag{4}$$

UNet-S is the updated segmentation network using the loss function defined by equation 4. Training was applied on 30 epochs and batch of 25 vertebra patches. Testing was applied on 792 vertebrae extracted from 172 test images manually. Evaluation was achieved by a metric called fit failure [14].

4) "Classification of Osteoporotic Vertebral Fractures Using Shape and Appearance Modelling": Diagnosing vertebral fracture was recognized and its severity level was determined based on measuring vertebral body heights [9]. The approach consists of modeling the format of the vertebrates' height in addition of k-nearest neighbour and random decision forests (RF) classifier for high quality segmentation of partial or full vertebrates of the body. Plain radiographs were used and tomography (CT) were computed. Fracture Size and shape was computed using statistical shape model (SSM) to achieve a linear model.

5) "Unfolded Cylindrical Projection for Rib Fracture Diagnosis": The approach introduced a new method for automatic rendering of unfolded clear view of the entire ribcage [15]. Segmentation detected anatomical landmarks using Random Forest (RF) classifier [16] that was trained by histogram of oriented gradients (HOG) [17] features. Using those detected landmarks, synthetic atlas was transformed to novel patient space for bounding the segmentation of the ribs. This was done by pre-defining a thorax box where everything outside it was discarded. Finally, an algorithm based on demon algorithm [18] was applied. According to results, the three wanted masks were warped: spine, sternum and ribs and removed other objects, which output a mask with mainly ribs and unrecognized objects like vessels and cables. Removing those vessels was made by using a vesselness filter [19].

6) "Automatic Localization of the Lumbar Vertebral Landmarks in CT Images with Context Features": The proposed framework had two modules [10]. One localized vertebral bodies and estimated their pose by detecting vertebral end plates in four steps, while the other localized key landmarks of vertebrae based on centers and pose predetermined in the first module. Two levels of Random Forest regression technique were applied [20]. During testing, a normally distributed probability map was constructed for every vertebral level and retrieved with the "Mean-Shift Mode-Seeking" algorithm [21]. Second, image deformation was done by curved planar reformation [22]. Re-slicing of CT-scans was done based on the curve that goes through the detected VB centers [23]. The second module was a separate localization of vertebral landmarks on each level of the lumbar spine from the five levels from L5 to L1. It had two successive layers of Random Forest regression techniques. The first layer was applied on appearance features while the second layer was on context features. Finally, regression was achieved by random forest per landmark [24]. The methods proposed were evaluated on a dataset of 28 CT images. The space between slices was 0.7 mm, and each slice size was 512x512. All images captured at least the S1-L1 levels, and, in some cases, the thoracic region captures up to level T10. There were five manual annotations made for every lumbar vertebra. One of them was the center of the VB. The other four were computed from the inferior articular process on a lumbar vertebra and include the bottom-left A and the bottom-right B, top-right C and the top-left$D$.

7) "Segmentation of Pathological Spines in CT Images Using a Two-Way CNN and a Collision-Based Model": The system introduces a two-way CNN architecture [3]. It was trained on images of normal spines. Image patches were extracted after choosing a center voxel randomly. The patches of size 27x27x27 and 55x55x55 were sent through to two different paths. The first path had nine convolutional layers and residual connections followed by a parametric rectified linear unit (PReLU).The second path had three convolutional layers followed by (PReLU) and a max-pooling layer repeatedly. Finally, a layer of a transposed convolution layer followed by a PReLU is applied to ensure that both paths have the same output size. The outputs were jointly sent to three fully connected layers and finally to a softmax function. Classification is done into three segmentation classes; anterior arch, posterior arch and background probabilities. The second step was initializing the collision-based model, which was a mesh union of two successive vertebrae (denoted as $M1$ and $M2$) with their computed mean pose and shape.

B. 3D Architecture

1) "Reconstruction of 3D Muscle Fiber Structure Using High Resolution Cryosectioned Volume": The initial phase was the correction of artifact which was a discontinuity of the color balance, discovered throughout the data and clearer in a projection view [25]. Therefore, artifact correction process was suggested to eliminate this discontinuity. An original image was $h(i,j,k)$ and its transform $H(x,y,z)$ were given and the high frequency area in the z-axis of the transformed image was zero-masked as defined in equation III-B1.

$$M(x,y,z) = \begin{cases} 0, & \text{if } \sqrt{x^2+y^2} < t_r \text{ and } |z| > t_z \\ 1, & \text{otherwise} \end{cases}$$

Where M was a zero-valued cylinder along z-axis, tr was radius of the cylinder. The cylinder is filled by ones in the range $-tz < z < tz$. tr and tz were experimented with values 0.2 and 0.08 respectively . The transform of the masked volume $F - 1(H(x,y,z)M(x,y,z))$, showed the effect of artifact correction on volume. Gradient-based structure tensor computed the muscle fiber local orientation around each voxel. Representing Gaussian multiplication respecting both the x and y axis for example. To make the photograph much smoother, another Gaussian multiplication was performed on

each element using a standard deviation $\sigma 2$. $\sigma 1$ was determined based on the noise that was contained in the given photograph.

2) "3D Cobb Angle Measurements from Scoliotic Mesh Models with Varying Face-Vertex Density": Detecting the severity level of the deformity or the damage in spine was done by measuring the cobb angle. Instead of measuring it from a 2D radiograph, this approach measured it from 3D constructed mesh [26]. 3D model for the spinal cord with alternating density per face to detect spinal deformity scoliosis which was abnormal curve in the spine. Unsupervised machine learning of vertebral column faces was used to locate the center of the vertebral column and detect the faces of the 3D mesh which was used for training.

Labeling and classifying contiguous faces of the mesh through Principle component analysis (PCA) were applied to convert the vertices from image to the mesh. Identifying and calculating the mesh faces were achieved by considering the vertebral shape was cylindrical and analyzing them to 3 groups. The superior endplate $F_{B,TOP}$, the inferior endplate $F_{B,BOTTOM}$ and the walls representing the vertebral surface $F_{B,SIDE}$. Unsupervised machine learning using k-means++ to classify the highest value cluster to $F_{B,TOP}$ and the lowest value cluster to $F_{B,BOTTOM}$. Then the faces of the mesh are classified into $F_{VB,TOP}$, $F_{VB,BOTTOM}$ and $F_{VB,SIDE}$. Linear classifier was responsible for grouping the contiguous faces of the same class and the group with the maximum number of faces was chosen to be the superior and interior endplates.

$$F_{SUP} = \underset{F_{A,j}}{\arg\max} \left(\text{count}\left(F_{A,j} \cap F_{B,TOP}\right)\right), \quad j = 1, 2, \ldots, J$$
$$F_{INF} = \arg\max \left(\text{count}\left(F_{A,j} \cap F_{B,BOTTOM}\right)\right), \quad j = 1, 2, \ldots, J \tag{5}$$

The 3D cobb angle was generated by constructing the superior endplate to the upper part of vertebrae and the inferior to the lower part of the vertebrae in which the deformity located. The parameters of these planes were calculated using the algorithm of random sample consensus (RANSAC) on both faces superior and inferior, ending up with normal vectors.

C. *Segmentation*

1) "Automatic Full Femur Segmentation from Computed Tomography Data-sets Using an Atlas-Based Approach": The target of this study was to demonstrate the automatic segmentation of the femur in clinical CTs to fully evaluate the health of the bone and to identify the impact of osteoporosis [27] . First, pre-processing was applied by re-sampling the CT scans to a resolution of 0.625mm by utilizing cubic interpolation. Afterwards, the scans volume were divided into two different sets, one included the right femur while the other include the left femur. Semi-automatic segmentation was done by graph-cut approach. In this approach, foreground (femur) and background (muscle, pelvis and tibia) regions were identified. MITK-GEM resulted in the creation of joint space in the segmented images. Therefore, the 6 MITK-GEM segmentations were afterwards manually improved and corrected by the aid of medical professionals.

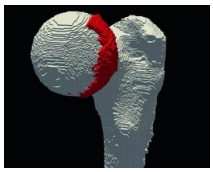

Fig. 4: Manual segmentation (white) overlaid with the MITK-GEM segmentation (red).

IV. Popular Databases

TABLE I: Databases used in previously mentioned papers.

Databases	No. of Samples	Specification
MURA Dataset [2]	40,561 images	Upper Limbs.
Osteoarthritis Initiative [28]	4,796 images	Right Knee.
SpineWeb [3]	300 images	Lumbar and Thoracolumbar Spine
Vertebrae Dataset [4]	296 images	Lateral Cervical Spine.
PACS [9]	9991 images	Thoracic and Lumbar Vertebrae.
CT Torso Dataset [11]	200 images	Human Torso.
Visible Korean Human [25]	11,015 images	Entire Human Body.
Femur CT Dataset [27]	500 images	Femur Bone.

V. Experimental Results

A. *"MURA: Large Dataset for Abnormality Detection in Musculoskeletal Radiographs"*

Cohen's kappa statistic was used to assess the model's accuracy compared with the radiologists 's [2]. On some areas as the wrist finger, the model achieved a score nearly close to the radiologists'accuracy. While on other parts as the forearm, humerus and shoulder, the model had the lowest score. Nonetheless, there were areas where the model did not achieve results as good as the best radiologist, but accomplished a better result than the worst radiologist, such as the elbow and hand. They used Receiver Operating Characteristic (ROC) to graph the model's specificity against sensitivity in comparison with the radiologists'. After the model predicted the abnormality possibility, a curve had been initialized from changing the threshold values used for the classification boundary. The performance of the radiologists lied above the curve, pointing out that the model was not as efficient to detect abnormalities relative to radiologists.

B. *"Segmentation of Pathological Spines in CT Images Using a Two-Way CNN and a Collision-Based Model"*

The performance of segmenting vertebrae [3] was measured by computing three different values. The first value is Dice similarity coefficient (DSC), and the second is mean symmetric surface distance (MSD)while the third is Hausdorff surface distance (HD). The mean $\pm$ standard deviation of the three computed measurements were 93.2$\pm$2.2%, 0.5$\pm$0.2mm, 8.4$\pm$3.4mm, respectively.

Fig. 5: Abnormal Image of an elbow from the MURA dataset that contains a medial epicondyle fracture.

C. "Shape-Aware Deep Convolutional Neural Network for Vertebrae Segmentation"

The introduction of the novel loss term in the training further reduced the average error by 12% achieving the best error of 0.99 pixels. A maximum average pixel-level segmentation accuracy of 97.01%, a Dice coefficient of 0.9438 and point to ground truth curve error < 1 pixel are achieved over the dataset. [4]

D. "Reconstruction of 3D Muscle Fiber Structure Using High Resolution Cryosectioned Volume"

Tractography on several muscles in the hips and head regions were computed, the results were the successful identification of each muscle fiber in the two given datasets. The female pelvis dataset showed 24 different muscles around the hips identifying each muscle with its name, and as for the male whole body dataset showed 4 masticatory muscles [25].

E. "Unfolded Cylindrical Projection for Rib Fracture Diagnosis"

A dataset [15] composed of 369 CT were used for landmark classifier training, and another CT dataset were used for testing. A clinical expert rated the specialized rib view on a Likert scale [15]. The scale values were: Gold - Diagnostic - Moderate - Low Level - Very Low Level of confidence. The testing chest scans were split to 44 known datasets and 26 unknown datasets. The qualitative evaluation resulted in 0.0% gold standard, 62.9% diagnostic confidence, 21.4% moderate confidence, 10.0% low-level of confidence, and 5.7% very low-level of confidence. Six cases from the seen database were manually labelled for a quantitative reference. They were separated as ribs and spine. The manually and automatically generated masks were compared resulting in high DICE, Sensitivity, Specificity values each.

F. "Automatic Localization of the Lumbar Vertebral Landmarks in CT Images with Context Features"

All images [10] were resampled to an isotropic spacing of 1x1x1mm. 20 images were randomly selected for training. A successfully detected VB center lies within 10mm from the respective manual annotation. The mean localization error, standard deviation and median value were 3.2 mm, 2.0mm and 2.8 mm respectively. Overall, the proposed method achieved mean localization error of 3.0 mm, with 1.6mm standard deviation and a median 2.7 mm. The localization errors under 6 mm were 95.4%. For the training of the second layer, experiments were done by removing randomly displaced ROIs of [24] instead using ROIs centered around the VB centers to increase localization error to $3.4 \pm 1.8mm$. The mean dice coefficient, across all the spinal levels was 88.8%.

G. "Automatic Full Femur Segmentation from Computed Tomography Data-sets Using an Atlas-Based Approach"

The MITK-GEM [27] approach was the best one so far that obtained a similarity coefficient of 0.99 and a Hausdorff distance of 4.5mm. In atlas-based approach, after eliminating the contralateral femur which resulted in the improvement of both the average Hausdorff distance and dice similarity coefficient. The average Hausdorff distance increased from 5.95mm to 8.53mm and the dice similarity coefficient decreased from 0.978 to 0.969 which is considered better results that they were.

H. "Automatic Knee Osteoarthritis Diagnosis from Plain Radiographs: A Deep Learning-based Approach"

Training the model on multicenter osteoarthritis study (MOST) dataset containing 3,026 subjects and tested by 3000 random samples of knee OA from Osteoarthritis Initiative (OAI) dataset containing 4,796 subjects. They [28] have reached an accuracy of Quadratic kappa coefficient of 0.83 and average multiclass accuracy of 66.71% .The diagnosis of radiological OA reached AUC (area under the curve) of 0.93 in a ROC (Receiver operator curve) curve.

I. "Classification of Osteoporotic Vertebral Fractures Using Shape and Appearance Modelling"

The accuracy [9] improved as the false positive decreased by 60% having sensitivity of 80%
. DXA manual annotations the false positive rate (FPR) decreased from 4.4% to 1.7% and the automated decreased from 12.7% to 8.8%. While CT manual annotations decreased from 8.9% to 3.3% , While the automated decreased from 9.7% to 7.0% . Reducing the automatic FPR by âL'Ĺ30% and the manual annotations by âL'Ĺ60%.

J. "3D Cobb Angle Measurements from Scoliotic Mesh Models with Varying Face-Vertex Density"

Testing is done [26] on 60 mesh models having adolescent idiopathic scoliosis (spinal deformity) triangular shaped with 48.8° mean cobb angle, in which each model is constructed from 17 varying face densities. Measuring the cobb angle with this semi-automated method even that the upper-end and lower-end of vertebral have to be manually selected, reaching an accuracy on faces having mean edge less than 6mm of 3.0° absolute mean error which is equivalent to 2.2° standard deviation.

TABLE II: The following table compare general and technical information for a number of databases.

Specification	Dataset	Results
Spinal disorders [3]	10 axially reconstructed CT images of the lumbar spine and thoracolumbar spine each for training and 15 axially reconstructed CT images of the lumbar spine for testing acquired from SpineWeb online platform.	DSC of 93.2±2.2%, MSD of 0.5±0.2mm and HD of 8.4±3.4mm
Lateral cervical spine [4]	296 real-life emergency room lateral cervical X-ray images. Trained on an augmented dataset of 26370 vertebrae, and tested on 792	The proposed framework had an average error of 1.11 pixels, and the introduction of the novel shape-aware term in the loss function scored an average error of 0.99 pixel
Rib fractures [15]	Clinically acquired, 369 CT datasets for landmark classifier training and 70 CT studies for testing.	The qualitative evaluation resulted in 0.0% gold standard, 62.9% diagnostic confidence, 21.4% moderate confidence, 10.0% low-level of confidence, and 5.7% very low-level of confidence.
Knee Osteoarthritis Diagnosis [28]	Training the model on multicenter osteoarthritis study (MOST) dataset containing 3,026 subjects and tested by 3000 random samples of knee OA from Osteoarthritis Initiative (OAI) dataset containing 4,796 subjects.	Quadratic kappa coefficient of 0.83 and average multiclass accuracy of 66.71% .The diagnosis of radiological OA reached AUC (area under the curve) of 0.93 in a ROC (Receiver operator curve) curve.
Osteoporotic Vertebral Fractures [9]	PACS collected CT scans for 868 patients of age 18 and older including thoracic (mid back) and lumbar (lower back) vertebrae scans.	The accuracy improved as the false positive decreased by 60% having sensitivity of 80%
Lumbar vertebral bodies [10]	28 lumbar-focused computed tomography images	Detection of landmarks with a mean localization error of 3.0 mm
Femoral fractures [27]	Three cadavers were scanned and resulted in the important bilateral hip CT scans. Resolution was 0.684x0.684mm with a thickness of 0.625mm. The CT scans contain the entire femur from the top of the iliac crest of the pelvis and ends in the proximal tibia.	The MITK-GEM approach was the best one so far that obtained a similarity coefficient of 0.99 and a Hausdorff distance of 4.5mm.
Hip joint and head regions [25]	Visible Korean Human was collected by the help of the Korea Institute of Science and Technology. It consists of 8506 images for the entire human body which were assembled mainly from the examination of cryosection of human corpses.	The successful identification of each muscle fiber in the two given datasets. The female pelvis dataset showed 24 different muscles around the hips and identifying each muscle with its name, and as for the male whole body dataset it showed 4 masticatory muscles.
Upper-limb extremity [2]	MURA contains 9,045 normal and 5,818 abnormal musculoskeletal radio-graphic studies of the upper extremity without any labels provided which help in identifying the exact abnormality in each x-ray image.	On some areas, the model's performance was comparable to the radiologists', while in other areas it still needed further improvement.

VI. CONCLUSION

Based on the summarized studies and the reviewed work and methods attempting to fill in gaps concerning detecting different abnormalities and musculoskeletal disorders, convolutional networks CNN is the most effective used method. Many approaches modified CNN as needed in order to execute the desired goal. Convolutional networks was used in different ways such as image segmentation and detecting abnormalities in different medical modalities, which is of our highest interest since it's closely related to the work we plan for in the near future.

VII. FUTURE WORK

Develop automatic expert systems that gain all the knowledge of experts and benefit from pattern recognition techniques. We aim to solve as much as possible of the problems unsolved by others and to improve accuracy. We should benefit from the experience gained from other researchers and make use of deep learning techniques as CNN. Different types of robust features will be applied to propose a reliable automatic system for musculoskeletal disorders detection and classification.

REFERENCES

[1] R. E. Marx, Bone and bone graft healing, Oral and maxillofacial surgery clinics of North America 19 (4) (2007) 455–466.

[2] P. Rajpurkar, J. Irvin, A. Bagul, D. Ding, T. Duan, H. Mehta, B. Yang, K. Zhu, D. Laird, R. L. Ball, et al., Mura dataset: Towards radiologist-level abnormality detection in musculoskeletal radiographs.

[3] R. Korez, B. Likar, F. Pernuš, T. Vrtovec, Segmentation of pathological spines in ct images using a two-way cnn and a collision-based model, in: International Workshop and Challenge on Computational Methods and Clinical Applications in Musculoskeletal Imaging, Springer, 2017, pp. 95–107.

[4] S. M. R. Al Arif, K. Knapp, G. Slabaugh, Shape-aware deep convolutional neural network for vertebrae segmentation, in: International Workshop and Challenge on Computational Methods and Clinical Applications in Musculoskeletal Imaging, Springer, 2017, pp. 12–24.

[5] A. Rasoulian, R. Rohling, P. Abolmaesumi, Lumbar spine segmentation using a statistical multi-vertebrae anatomical shape+ pose model, IEEE transactions on medical imaging 32 (10) (2013) 1890–1900.

[6] I. Castro-Mateos, J. M. Pozo, M. Pereañez, K. Lekadir, A. Lazary, A. F. Frangi, Statistical interspace models (sims): application to robust 3d spine segmentation, IEEE transactions on medical imaging 34 (8) (2015) 1663–1675.

[7] D. E. Beaton, C. Bombardier, D. C. Cole, S. Hogg-Johnson, D. Van Eerd, C. E. Group, A pattern recognition approach to the development of a classification system for upper-limb musculoskeletal disorders of workers, Scandinavian journal of work, environment & health (2007) 131–139.

[8] B. J. Schwaiger, A. S. Gersing, J. Mbapte Wamba, M. C. Nevitt, C. E. McCulloch, T. M. Link, Can signal abnormalities detected with mr imaging in knee articular cartilage be used to predict development of morphologic cartilage defects? 48-month data from the osteoarthritis initiative, Radiology 281 (1) (2016) 158–167.

[9] P. A. Bromiley, E. P. Kariki, J. E. Adams, T. F. Cootes, Classification of osteoporotic vertebral fractures using shape and appearance modelling, in: International Workshop and Challenge on Computational Methods and Clinical Applications in Musculoskeletal Imaging, Springer, 2017, pp. 133–147.

[10] D. Damopoulos, B. Glocker, G. Zheng, Automatic localization of the lumbar vertebral landmarks in ct images with context features, in: International Workshop and Challenge on Computational Methods and Clinical Applications in Musculoskeletal Imaging, Springer, 2017, pp. 59–71.

[11] J. W. Kung, J. S. Wu, S. K. Shetty, V. C. Khasgiwala, P. Appleton, M. G. Hochman, Spectrum and detection of musculoskeletal findings on trauma-related ct torso examinations, Emergency radiology 21 (4) (2014) 359–365.

[12] J. Deng, W. Dong, R. Socher, L. jia Li, K. Li, L. Fei-fei, Imagenet: A large-scale hierarchical image database.

[13] A. Tiulpin, J. Thevenot, E. Rahtu, S. Saarakkala, A novel method for automatic localization of joint area on knee plain radiographs, in: Scandinavian Conference on Image Analysis, Springer, 2017, pp. 290–301.

[14] P. Bromiley, J. Adams, T. Cootes, Localisation of vertebrae on dxa images using constrained local models with random forest regression voting, in: Recent Advances in Computational Methods and Clinical Applications for Spine Imaging, Springer, 2015, pp. 159–171.

[15] C. Tobon-Gomez, T. Stroud, J. Cameron, D. Elcock, A. Murray, D. Wyeth, C. Conway, S. Reynolds, P. A. G. Teixeira, A. Blum, et al., Unfolded cylindrical projection for rib fracture diagnosis, in: International Workshop and Challenge on Computational Methods and Clinical Applications in Musculoskeletal Imaging, Springer, 2017, pp. 36–47.

[16] A. Criminisi, J. Shotton, Decision forests for computer vision and medical image analysis, Springer Science & Business Media, 2013.

[17] N. Dalal, B. Triggs, Histograms of oriented gradients for human detection, in: Computer Vision and Pattern Recognition, 2005. CVPR 2005. IEEE Computer Society Conference on, Vol. 1, IEEE, 2005, pp. 886–893.

[18] W. Crum, L. Griffin, D. Hill, D. Hawkes, Zen and the art of medical image registration: correspondence, homology, and quality, NeuroImage 20 (3) (2003) 1425–1437.

[19] A. F. Frangi, W. J. Niessen, K. L. Vincken, M. A. Viergever, Multiscale vessel enhancement filtering, in: International Conference on Medical Image Computing and Computer-Assisted Intervention, Springer, 1998, pp. 130–137.

[20] B. Glocker, D. Zikic, E. Konukoglu, D. R. Haynor, A. Criminisi, Vertebrae localization in pathological spine ct via dense classification from sparse annotations, in: International Conference on Medical Image Computing and Computer-Assisted Intervention, Springer, 2013, pp. 262–270.

[21] Y. Cheng, Mean shift, mode seeking, and clustering, IEEE transactions on pattern analysis and machine intelligence 17 (8) (1995) 790–799.

[22] A. Kanitsar, D. Fleischmann, R. Wegenkittl, P. Felkel, M. E. Gröller, Cpr: curved planar reformation, in: Proceedings of the conference on Visualization'02, IEEE Computer Society, 2002, pp. 37–44.

[23] A. Kanitsar, D. Fleischmann, R. Wegenkittl, P. Felkel, M. E. Gröller, Cpr: curved planar reformation, in: Proceedings of the conference on Visualization'02, IEEE Computer Society, 2002, pp. 37–44.

[24] Y. Gao, D. Shen, Context-aware anatomical landmark detection: application to deformable model initialization in prostate ct images, in: International Workshop on Machine Learning in Medical Imaging, Springer, 2014, pp. 165–173.

[25] Y. Otake, K. Miyamoto, A. Ollivier, F. Yokota, N. Fukuda, L. J. OâĂŹDonnell, C.-F. Westin, M. Takao, N. Sugano, B. S. Chung, et al., Reconstruction of 3d muscle fiber structure using high resolution cryosectioned volume, in: International Workshop and Challenge on Computational Methods and Clinical Applications in Musculoskeletal Imaging, Springer, 2017, pp. 85–94.

[26] K. R. P. S. K. S. . V. T. PetkoviÄĞ, U., 3d cobb angle measurements from scoliotic mesh models with varying face-vertex density, in: International Workshop and Challenge on Computational Methods and Clinical Applications in Musculoskeletal Imaging, Springer, 2017, pp. 48–58.

[27] B. A. Besler, A. S. Michalski, N. D. Forkert, S. K. Boyd, Automatic full femur segmentation from computed tomography datasets using an atlas-based approach, in: International Workshop and Challenge on Computational Methods and Clinical Applications in Musculoskeletal Imaging, Springer, 2017, pp. 120–132.

[28] A. Tiulpin, J. Thevenot, E. Rahtu, P. Lehenkari, S. Saarakkala, Automatic knee osteoarthritis diagnosis from plain radiographs: a deep learning-based approach, Scientific reports 8 (1) (2018) 1727.